OPEN ACCESS
IOP Publishing
Plasma Sources Science and Technology
Plasma Sources Sci. Technol. **34** (2025) 085014 (9pp)
https://doi.org/10.1088/1361-6595/adfc0a

Dynamics of electron power absorption in capacitive radio-frequency CF_4 plasmas operating in the striation mode

Zhenhua Zhou[1,8], Xiaokun Wang[2,8], Hanyang Li[3], Dong Yang[3], Wenjin Zhang[3], Julian Schulze[2], Peter Hartmann[4], Zoltán Donkó[4], Yongxin Liu[5] and Yangyang Fu[3,6,7,*]

[1] Department of Engineering Physics, Tsinghua University, Beijing 100084, People's Republic of China
[2] Chair of Applied Electrodynamics and Plasma Technology, Department of Electrical Engineering and Information Sciences, Ruhr University Bochum, 44801 Bochum, Germany
[3] Department of Electrical Engineering, Tsinghua University, Beijing 100084, People's Republic of China
[4] Institute for Solid State Physics and Optics, HUN-REN Wigner Research Centre for Physics, 1121 Budapest, Hungary
[5] Key Laboratory of Materials Modification by Laser, Ion, and Electron Beams (Ministry of Education), School of Physics, Dalian University of Technology, 116024 Dalian, People's Republic of China
[6] State Key Laboratory of Power System Operation and Control, Department of Electrical Engineering, Tsinghua University, Beijing 100084, People's Republic of China
[7] Sichuan Energy Internet Research Institute, Tsinghua University, Sichuan 610213, People's Republic of China

E-mail: fuyangyang@tsinghua.edu.cn

Received 21 May 2025, revised 18 July 2025
Accepted for publication 15 August 2025
Published 29 August 2025

Abstract

The dynamics of the electron power absorption in radio-frequency CF_4 capacitively coupled plasmas operating in the striation mode is investigated based on a particle-in-cell/Monte Carlo collision model. In the striation mode, the mean electron energy within the bulk plasma exhibits a spatially modulated structure with high-energy peaks. Using the Boltzmann term analysis method, we demonstrate that non-local collisional power absorption, rather than Ohmic heating, dominates the formation of these peaks. Through test particle trajectory calculations, we demonstrate that most of the energetic electrons can traverse the spatially modulated electric field and this transportation process is responsible for most of the non-local collisional power absorption. Some low-energy electrons undergo multiple rebounds and are confined within the spatially modulated field; however, the power absorption by these electrons is negligible compared to ones capable of passing through the modulated field.

Keywords: electron power absorption, CF_4 capacitively coupled plasma, striation mode, particle-in-cell simulation

[8] These authors contributed equally to this work.
[*] Author to whom any correspondence should be addressed.

Original Content from this work may be used under the terms of the Creative Commons Attribution 4.0 licence. Any further distribution of this work must maintain attribution to the author(s) and the title of the work, journal citation and DOI.

© 2025 The Author(s). Published by IOP Publishing Ltd

1. Introduction

Low-temperature radio-frequency (RF) capacitively coupled plasmas (CCPs) are widely used in semiconductor processing applications including plasma etching, deposition, and surface modification [1, 2]. CF_4 is one of the most commonly used electronegative gases in CCP-based etching processes, which can generate various reactive species, such as CF_x radicals, particularly useful for plasma etching processing [3, 4]. Precise control of key etching process parameters, such as the ion flux [5] and ion energy distribution [6], is essential. Therefore, a fundamental understanding of RF CCPs operating in CF_4 is crucial for ensuring the precision and selectivity required by modern etching techniques [7–9].

In CCPs, the discharge mode refers to the specific mechanism by which a plasma is generated and sustained by the applied external power. In addition to the two common operation modes of RF CCPs, the α mode [10, 11] and the γ mode [12–14], the other two specific discharge operation modes can be observed in electronegative RF capacitive discharges: the drift-ambipolar (DA) mode [15, 16] and the striation mode [17–20]. The DA mode is characterized by a drift electric field built up in the bulk region and an ambipolar electric field built up near the sheath edges. In this mode, the quasineutrality of the bulk region is primarily maintained by positive and negative ions. The electron density within the bulk plasma is depleted due to the strong electronegativity. At both sheath edges, electrons exhibit localized density peaks, leading to the formation of ambipolar electric fields there [15].

The striation mode typically develops at relatively low driving frequencies [19] or under specific voltage conditions [18] and is characterized by the formation of spatially periodic 'comb-like' plasma density structures. In this mode, positive and negative ions can respond to the RF electric field. This rebuilds the local polarity of the space charge, ultimately leading to a spatially alternating enhancement or weakening of the local electric field in the bulk plasma [21]. These discharge modes modulate the electric field structures, which, in turn, affect electron power absorption in the electric field. Notably, 'electron power absorption' involves accelerating electrons within an electric field where they absorb energy. Conversely, 'electron heating' refers to the isotropization of electron kinetic energy, or an increase in electron temperature resulting from power absorption after collision processes [10].

Studying the electron power absorption mechanism of CCPs is essential for optimizing plasma processes due to the rapid response of electrons to electric fields. In CCPs, electron power absorption directly influences the ionization rate and the production of reactive species, both of which are critical for etching and deposition processes [10, 22, 23]. Previous studies have extensively investigated the electron power absorption mechanisms of CF_4 RF capacitively coupled discharge systems driven by single-frequency [24], dual-frequency [25], and tailored voltage waveforms [26]. These electron power absorption mechanisms have also been studied in CF_4 CCPs operating in DA mode [16] and striation mode [24]. The effects of various discharge parameters, including the gas pressure, driving frequency and RF power [27], as well as the gap distance and secondary electron emission [16], on the electron power absorption process involving CF_4 CCPs have been discussed. Regarding CF_4 capacitive RF discharges operated in the striation mode, the spatiotemporal characteristics of electron power absorption have been investigated [24]. In the striation mode, strong non-local collisional power absorption (previously known as stochastic heating [28–30]) occurs in the bulk plasma region, presenting periodic patterns with alternating heating and cooling in space [24]. However, the underlying physics of electron dynamics in power absorption remains unclear. For instance, the mechanisms by which electrons are transported among striations and how this ultimately leads to non-local collisional power absorption in the bulk plasma remain unclear.

In this work, based on a particle-in-cell/Monte Carlo collision (PIC/MCC) model, we investigate the dynamics of the electron power absorption in CF_4 capacitive RF discharges operating in the striation mode. According to calculations implemented via the Boltzmann term analysis method, we reveal that the bulk plasma exhibits a spatially modulated electron energy profile, where non-local collisional power absorption dominates over Ohmic power absorption in shaping the spatially modulated electron energy profile. The evolution of the spatially modulated electric field periodically compresses and expands the electron fluid, which ensures the existence of the non-local collisional power absorption mechanism in the bulk plasma. We conduct a further investigation of the electron dynamics of power absorption through test particle trajectory calculation. We confirm that, under the conditions studied, most electrons can traverse the spatially modulated region and fully engage in power absorption along their trajectories. A subset of low-energy electrons undergoes multiple rebounds in the striated electric field, which confines them. However, much less power absorption occurs during the process. Additionally, this electron confinement results in a spatially modulated electron density structure.

This paper is organized as follows. Section 2 provides detailed descriptions of the simulation approach and the Boltzmann term analysis method. Section 3 presents the results of a comparison between striation mode and DA mode discharges, focusing on their mean electron energy profile characteristics. An analysis is then conducted on the electron power absorption mechanism. Finally, in section 4, conclusions are drawn.

2. Model and method

2.1. Simulation method

The results presented in this work are obtained with an electrostatic PIC/MCC code in one spatial dimension and three velocity dimensions (1d3v), which has been validated against experiments [21]. The charged particles included in the simulations are CF_3^+, CF_2^+, CF_3^-, F^- ions and electrons.

Table 1. Control parameters applied in the simulations and the resulting discharge operation mode. $T_g = 350$ K, $V_0 = 300$ V.

Case No.	$[p, d, f]$	Discharge Mode
1	[60 Pa, 2 cm, 6.78 MHz]	STR
2	[60 Pa, 2 cm, 13.56 MHz]	DA
2	[60 Pa, 2 cm, 27.12 MHz]	DA

Electron–neutral collision processes, including elastic scattering, vibrational excitation, electronic excitation, dissociative ionization, neutral dissociation and attachment, are considered in this work. Additionally, the ion-neutral collision processes (both positive and negative) include elastic scattering, dissociative ionization and neutral dissociation. The recombination processes of positive ions with electrons and negative ions are also considered. More information about the aforementioned collision processes and their corresponding cross sections can be found in [24]. Under the conventional parallel electrode geometry, a powered electrode is driven by an RF voltage source $V_0\cos(2\pi ft)$, whereas a grounded electrode is set at the other side. The background CF_4 gas pressure p, gas temperature T_g, gap distance d, voltage amplitude V_0, and driving frequency f, as well as the corresponding discharge modes, are presented in table 1. These control parameters are selected for a comparative analysis of striation mode and DA mode CF_4 capacitive discharges. Surface interactions, including elastic electron reflection at a constant coefficient $R = 0.7$ and secondary electron emissions induced by positive ion bombardment with a constant coefficient $\gamma = 0.01$, are applied at both electrodes [31]. It was previously validated that this electron reflection coefficient leads to relatively accurate simulation results for stainless steel electrodes [32]; the secondary electron emission coefficient applied in this work has also been experimentally verified in [31]. A spatial resolution of $\Delta x = d/1000$ and a temporal resolution of $\Delta t = 1/8000\,f$ are used to ensure the stability and precision of the simulation.

2.2. Boltzmann term analysis

We employ the Boltzmann term analysis method to provide a spatiotemporally resolved description of the electron power absorption process [33–35]. This first-principle method has been extensively used for investigating the electron power absorption mechanisms of capacitive RF discharges. Details of this approach can be found in an earlier work [36], and only the most important concepts are provided here for simplicity. By rearranging the first moment equation of the 1D Boltzmann equation for electrons, one can obtain the expression of the total electric field E with its components:

$$E = E_{\mathrm{in}} + E_{\nabla p} + E_{\mathrm{Ohm}}, \tag{1}$$

where

$$E_{\mathrm{in}} = -\frac{m_e}{en_e}\left[\frac{\partial}{\partial t}\left(n_e u_e\right) + \frac{\partial}{\partial x}\left(n_e u_e^2\right)\right], \tag{2}$$

$$E_{\nabla p} = -\frac{1}{en_e}\frac{\partial}{\partial x}p_{xx}, \tag{3}$$

$$E_{\mathrm{Ohm}} = \frac{\Pi_{\mathrm{coll}}}{en_e}. \tag{4}$$

Here, m_e is the electron mass, e is the unit charge, n_e is the electron density, u_e is the mean electron velocity, and p_{xx} represents the diagonal component of the electron pressure tensor. Π_{coll} is the electron momentum change induced by collisions [37], given by

$$\Pi_{\mathrm{coll}} = -n_g m_e \int v_e v_{ex} f_e \sigma_m \mathrm{d}^3\boldsymbol{v}, \tag{5}$$

where n_g is the gas density, v_e and v_{ex} are the electron velocity and its component in x-direction, f_e is the electron distribution function, and σ_m is the effective electron momentum transfer collision cross section. Each term on the right-hand-side of equation (1) corresponds to a distinct physical mechanism. The inertia term, E_{in}, corresponds to the electric field required to balance the electron momentum changes. The Ohmic term, E_{Ohm}, arises from collisions between electrons and particles of the background gas. The pressure gradient term, $E_{\nabla p}$, denotes the electric field originating from the electron pressure gradient.

The total electron power absorption and its components can be obtained by multiplying equation (1) with the electron current density $J_e = -en_e u_e$, where u_e is the mean electron velocity in the x-direction obtained directly from the simulations. After multiplying, the term E_{Ohm}, which corresponds to the field that balances the electron momentum transfer process due to collisions, is defined as the Ohmic power absorption term

$$P_{\mathrm{Ohm}} = J_e E_{\mathrm{Ohm}}. \tag{6}$$

The sum of the other terms is then defined as non-local collisional power absorption, P_{nc}, which was previously known as stochastic heating [28–30]:

$$P_{\mathrm{nc}} = J_e\left(E_{\mathrm{in}} + E_{\nabla p}\right). \tag{7}$$

3. Results and discussion

In RF discharges, the electron power absorption in the electric field eventually affects the electron energy. Figure 1 presents the spatiotemporal distributions of the mean electron energy, $\mathcal{E}_e$, of the CF_4 capacitive RF discharge operated in striation mode in (a) case 1 and DA mode in (b) case 2 and (c) case 3. In striation mode (panel (a)), high-energy electrons are concentrated in the bulk plasma region, where modulation of $\mathcal{E}_e$ can be observed in space. In panels (b) and (c), the striation structures in the bulk plasma disappear, leaving only clustered high-energy regions. To illustrate these differences more clearly, the spatial profiles of the mean electron energy at the RF phase of $t/T = 0.35$ in figures 1(a)–(c), are presented in figure 2(a). The value of 0.35 is chosen for the appearance of striations. It can be clearly observed that $\mathcal{E}_e$ near the midplane $x/d = 0.5$ in the striation mode (red line) presents the spatially modulated energy peaks. To clarify, figure 2(b) shows the spatial profile of the electron power absorption P_e at $t/T = 0.35$, which corresponds to figure 2(a). Similar treatment of a cut

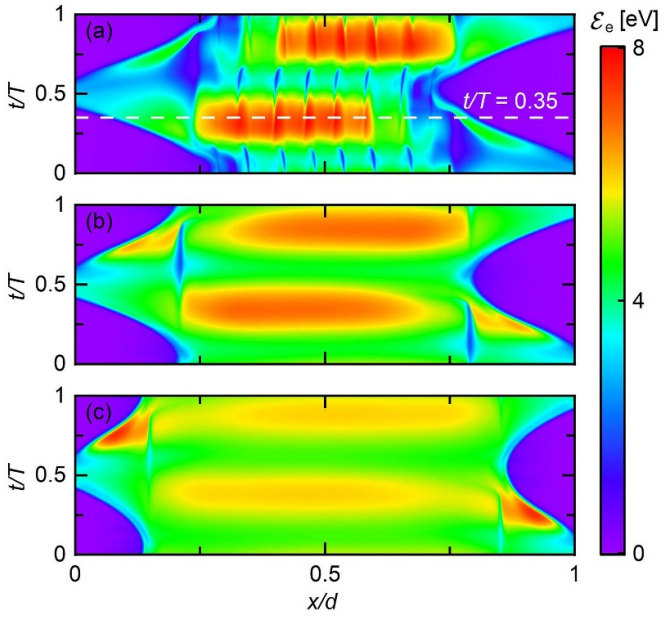


Figure 1. Spatiotemporal distributions of the mean electron energy $\mathcal{E}_e$ in the CF_4 capacitive RF discharges in (a) case 1, (b) case 2 and (c) case 3 (see table 1). The discharge operated in the (a) striation mode yields a significantly higher $\mathcal{E}_e$ in the bulk region than does the discharge in the (b)(c) DA mode.

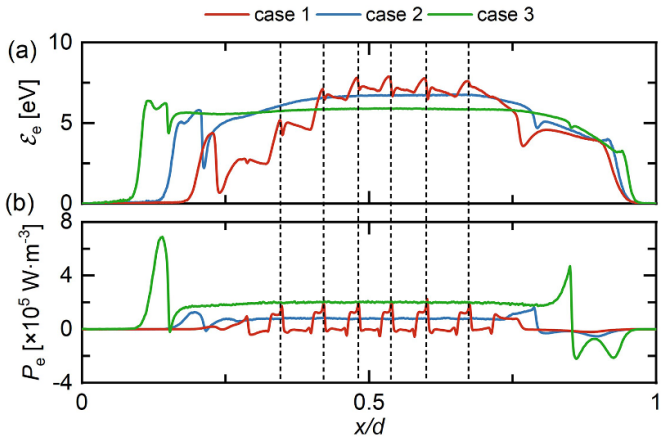


Figure 2. Spatial profiles of (a) the mean electron energy $\mathcal{E}_e$ and (b) the electron power absorption P_e in cases 1−3 at RF phase $t/T =$ 0.35 shown in figure 1. The position of the electron energy peak in case 1 corresponds exactly to the power absorption peak.

of P_e at a given t, can be found in previous work [18]. In panel (b), the locations of P_e peaks in the striation mode correspond to the peaks of the mean electron energy in panel (a), as indicated by the black dashed lines. This indicates that electron energy power absorption directly causes energy peak formation.

To further investigate the mechanism contributing to the formation of the striated electron energy profile, we apply the Boltzmann term analysis method. Figure 3 shows the spatial distributions of the RF averaged total electron power absorption levels P_e and their components P_{in}, $P_{\nabla p}$ and P_{Ohm}, where panels (a), (b) and (c) correspond to cases 1, 2 and 3, respectively. The agreement of $P_e = J_e E$ (obtained directly from the simulation, red line) and the summation of its component terms

$$P_{tot} \equiv J_e \left(E_{in} + E_{\nabla p} + E_{Ohm}\right) \tag{8}$$

(blue dashed line) validates the Boltzmann term analysis method applied here. Notably, the minor difference between P_e (from PIC) and P_{tot} (from Boltzmann term analysis) is due to the assumption of Maxwellian electron energy distribution function while estimating the electron momentum loss for calculating E_{Ohm}. Figure 3(a) shows that, in the striation mode, peaks are observed in the total electron power absorption (P_e, red line), where the pressure gradient power absorption ($P_{\nabla p}$, green line) dominates at the corresponding positions. In contrast, Ohmic power absorption (P_{Ohm}, purple line) is weaker in these regions. The contribution of the third term, P_{in}, is negligible. Therefore, we can conclude that non-local collisional power absorption P_{nc} (defined in equation (7)), which includes $P_{\nabla p}$, dominates the formation of the power absorption peaks in the striation mode rather than Ohmic power absorption P_{Ohm}. In the DA mode, however, the RF averaged P_e in the bulk region is almost completely contributed by Ohmic power absorption P_{Ohm}, as presented in figures 3(b) and (c). It can therefore be suggested that, in CF_4 CCPs operated in the striation mode, non-local collisional power absorption within the bulk region is enhanced, which contributes to the formation of striated spatial distributions of the mean electron energy.

The spatiotemporal distributions of the electron power absorption through Ohmic power absorption P_{Ohm} and non-local collisional power absorption P_{nc} in cases 1~3 are given in figures 4(a1)–(c1) and (a2)–(c2), respectively. The first row of figure 4 shows that P_{Ohm} within the bulk region increases as f increases. Ohmic power absorption is characterized by the acceleration of electrons within the drift electric field existing in the bulk plasma [1, 3]. The subsequent collisions of these accelerated electrons with neutrals result in electron momentum transfers, which ultimately lead to the electron drift velocity being transformed into a thermal velocity, ultimately inducing an increase in the electron temperature. With respect to non-local collisional power absorption, in panel (a2), P_{nc} of the striation mode within the bulk region presents a comb-like distribution with alternating energy gain and loss in space. As a comparison, as presented in panels (b2) and (c2), the levels of P_{nc} in the DA mode are almost negligible in the bulk region compared with that in the striation mode (shown in panel (a2)) but significantly greater at the plasma-sheath edge. Non-local collisional power absorption, as firstly demonstrated by Godyak *et al* [38, 39], is driven mainly by the interactions between the electrons and oscillating electric fields at the plasma-sheath edge in an electropositive CCP discharge. Electrons can be decelerated and then reflected by the sheath electric field; then, they undergo energy gain and loss during the expansion and collapse phases of an RF sheath,

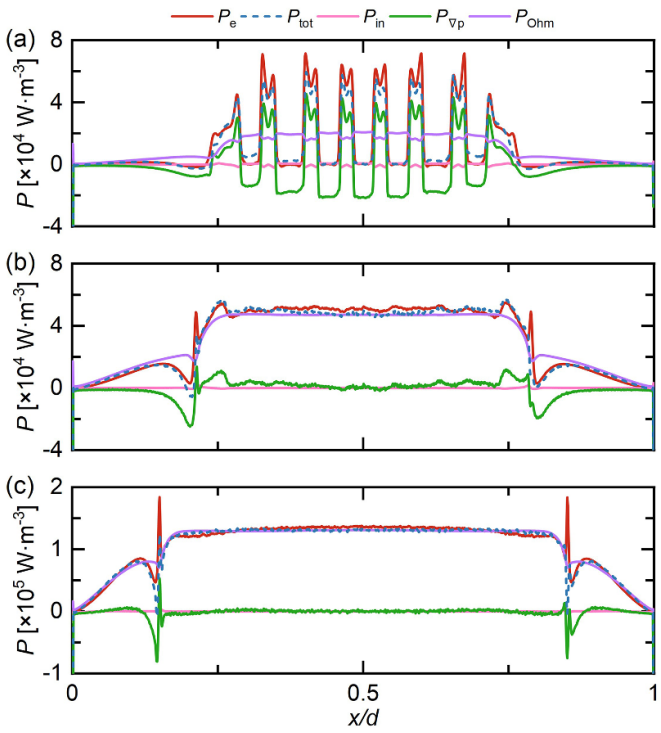


Figure 3. Spatial profiles of the RF averaged electron power absorption P_e and the contributions of its component terms (P_{in}, $P_{\nabla p}$ and P_{Ohm}) in the CF_4 capacitive RF discharges of (a) case 1, (b) case 2 and (c) case 3. The sum of the above component terms, P_{tot} (blue dashed line), exhibits agreement with P_e (red line). The agreement validates the Boltzmann term analysis method applied in this work. In (a), $P_{\nabla p}$ (green line) is the main term contributing to the peaks in the total electron power absorption P_e, while P_{Ohm} is the main contribution term in (b) and (c).

respectively. Therefore, the completion of non-local collisional power absorption is dependent on electron non-local kinetic processes and requires additional electron–neutral collisions to induce an increase in the electron temperature [28–30]. In the CF_4 CCPs operated in the DA mode, non-local collisional power absorption is also significant at the plasma-sheath edge, as illustrated in panels (b2) and (c2), similar to the results obtained for conventional electropositive CCPs. Near the sheath, vertical regions of non-local collisional power absorption can also be observed in panels (b2) and (c2); this results from the ambipolar field created by the electron density peaks in the DA mode there [16]. However, for the striation mode illustrated in panel (a1), non-local collisional power absorption also occurs in the bulk region, presenting a spatially modulated profile.

To further clarify the electron kinetics of such a non-local collisional power absorption enhancement in a bulk plasma, we apply test particle trajectory calculations [40, 41]. Based on the spatiotemporal distribution of the electric field E given by the simulation, this method calculates the trajectory of a test electron with the given initial condition, (x_0, t_0, v_0), by solving Newton's equation at each time step and neglecting any electron collisions along the trajectory. Additionally, the calculations do not consider the thermal motion of the test electron. Figure 5(a) shows the trajectories of two test electrons that start at $(x_0, t_0, v_0) = (0.5d, 0.33T, 0)$ (brown trajectory) and $(0.75d, 0.35T, 0)$ (green trajectory), respectively, within the spatiotemporally resolved electric field E obtained in case 1. These two initial conditions are chosen to demonstrate two characteristic single-particle trajectories. The black dashed lines represent the spatiotemporal evolution trends of the plasma-sheath edge locations on both sides [42]. In the brown trajectory, the test electron is trapped via multiple rebounds ($t/T = 0.33 \sim 0.55$). Figure 5(c) provides a zoomed-in view of panel (a) to help understand electron confinement. The electric field exhibits a spatially modulated structure that alternates between positive and negative polarities. The red area indicates the region where $E(x,t) > 0$, driving the test electron to be transported toward the $x/d = 0$ side. In contrast, the blue area represents $E(x,t) < 0$, inducing the test electrons to move toward the $x/d = 1$ side. Thus, electron confinement occurs mainly at transitions in the electric field's polarity. In panel (c), the test electron first enters the red area and moves downward. Then, the electron enters the blue area and moves upward. This process repeats and eventually leads to the rebound process. Since the electric field is stronger in the red region than in the blue region, the test particle completes the rebound process more quickly there. Thus, the trajectory is mainly located in the blue region. Panel (b) shows the corresponding temporal evolution of the kinetic energy $\mathcal{E}_{ek} = m_e v_e^2/2e$. During confinement, the kinetic energy of the test electron intermittently increases but remains less than 1 eV. After exiting the striation region, the test electron accelerates, undergoing rebounding between the sheath edge and the striations ($t/T = 0.55 \sim 1$). For the green trajectory, the test electron begins at the plasma-sheath edge, with an initial position of $x/d = 0.75$ and travels toward $x/d = 0$. This motion is driven by the electric field in the bulk plasma. As shown in figure 5(b), the test electron of the green trajectory is accelerated to obtain a kinetic energy $\mathcal{E}_{ek}$ of approximately 2 eV by the sheath expansion ($t/T = 0.35 \sim 0.36$). Once it reaches this kinetic energy, the test electron is no longer trapped among the striations. Thus, it can travel through the bulk region and undergo alternating accelerations and decelerations. This results in a spatially modulated $\mathcal{E}_{ek}$ within the bulk plasma along the trajectory ($t/T = 0.36 \sim 0.42$). In general, low-energy electrons can be confined within the bulk region by triggering multiple rebounds in the spatially modulated electric field. The other electrons exhibit a striated spatial profile of their energy while traveling through the bulk region.

In order to investigate the role of the above mentioned electron dynamics on the relevant spatiotemporal behavior, figure 6 presents a zoomed-in view of the (a) electron density n_e, (b) electric field E, (c) non-local collisional power absorption P_{nc} and (d) Ohmic power absorption P_{Ohm} obtained in case 1. The black dashed region in panel (b) indicates the transition of the polarity of the field, inducing the confinement of the electrons as introduced in figure 5(c). This confinement directly leads to the formation of electron density peaks, as one can observe in panel (a). Furthermore, due to the confinement effect, these electrons have a rather low drift velocity. Since Ohmic power absorption is controlled by the electron drift motion, P_{Ohm} is weakened where electrons are trapped, as

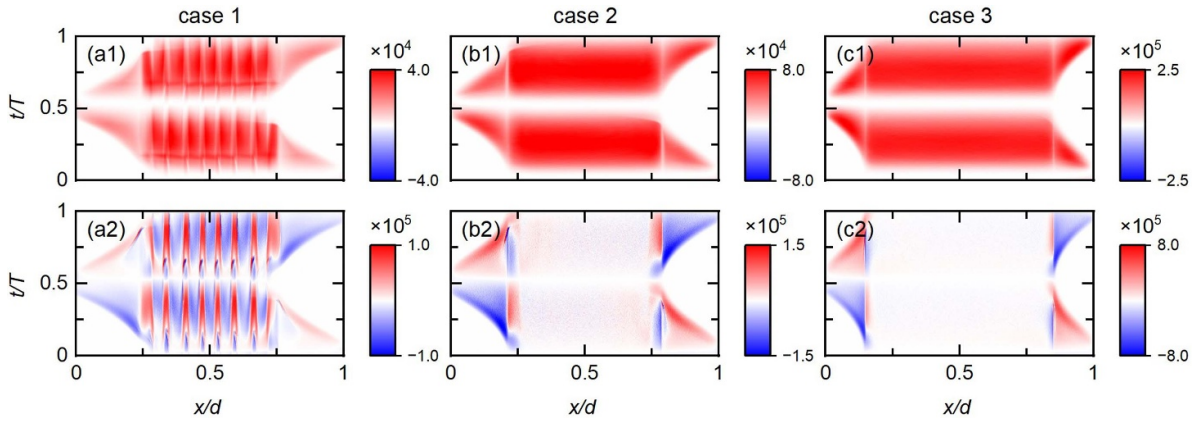


Figure 4. Spatiotemporal distributions of the electron power absorption [W·m^{-3}] through (a1)–(c1) Ohmic power absorption and (a2)–(c2) non-local collisional power absorption in (a) case 1, (b) case 2 and (c) case 3, respectively. In (a2), $P_{\rm nc}$ of the striation mode has spatially modulated structures consisting of energy gain and loss in the bulk region. In (b2) and (c2), $P_{\rm nc}$ is much weaker in the plasma bulk of the DA mode.

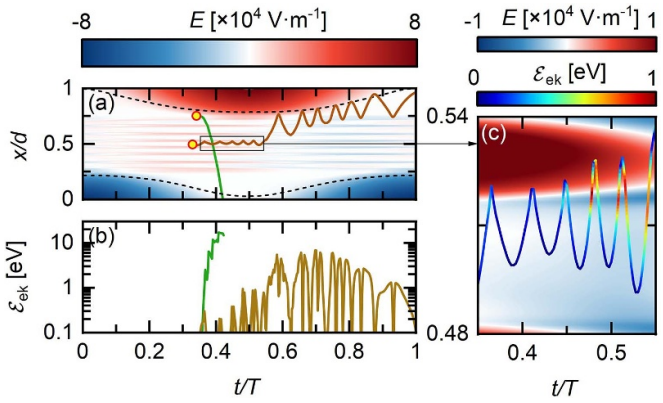


Figure 5. (a) Two trajectories of test electrons in the electric field E obtained in case 1 (striation mode). The green and brown trajectory are initialized at $(x_0, t_0, v_0) = (0.5d, 0.33T, 0)$ and $(0.75d, 0.35T, 0)$, respectively. (b) Temporal evolution of the corresponding electron kinetic energy $\mathcal{E}_{\rm ek} = m_{\rm e}v_{\rm e}^2/2e$. (c) Zoomed-in view of the brown trajectory in panel (a). The evolution of $\mathcal{E}_{\rm ek}$ is color coded along the trajectory. The test electron of the brown trajectory is confined between the spatially modulated field structure, which is achieved by the rebound of electrons between positive and negative electric fields. Regarding the green trajectory, the test electron travels across the bulk region, where $\mathcal{E}_{\rm ek}$ exhibits a striated temporal evolution.

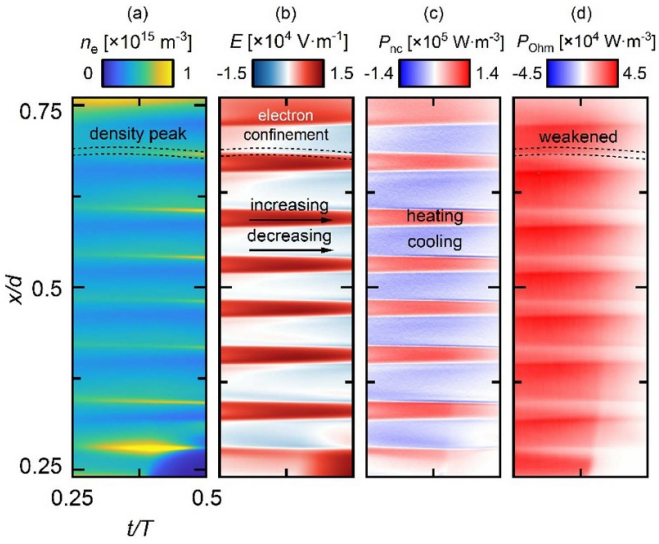


Figure 6. Zoomed-in view of the spatially modulated region of (a) electron density $n_{\rm e}$, (b) electric field E, (c) non-local collisional power absorption $P_{\rm nc}$ and (d) Ohmic power absorption $P_{\rm Ohm}$ obtained in case 1. The alternating positive and negative polarity of the spatially modulated electric field in panel (b) (black dashed line) can induce confinement of electrons, as introduced by test electron calculations in figure 5(c). On the other hand, the temporal evolution of the spatial modulation structure of the electric field, will lead to non-local collisional power absorption and cooling, respectively.

presented in panel (d). Additionally, as marked by the arrows in panel (b), the increase and decrease of the spatially modulated electric field over time will finally lead to the compression and expansion of the electron fluid, respectively. This is similar to the effect induced by the oscillation of sheaths. Since the green test electron trajectory presented in figure 5 traverses across the entire bulk region, it undergoes non-local collisional power absorption along its trajectory. Additionally, the electron also reaches a sizable drift velocity, therefore considerable Ohmic power absorption also occurs during transport. In contrast, the brown test electron trajectory in figure 5 undergoes a very small increase in energy (<1 eV), and less power absorption occurs in this trajectory.

Figure 7(a) gives the spatiotemporal distribution of $n_{\rm e}$ in case 1. There are high-density peaks at the maximum sheath width (e.g. $x/d = 0.25$), and between these peaks there is a striated spatial structure of the electron density. We consider the electron dynamics departing from $x/d = 0.25$ and 0.5 to be representative. These two positions represent the electrons at the density peak at the maximum sheath width, and in the bulk plasma region, respectively. In order to further explore the importance of the two electron dynamic processes dominating the discharge in figure 5, more test particle calculations are carried out. Trajectories of ten test particles departing from $x/d = 0.25$ and at different initial RF phases are presented in figure 7(b). The kinetic energy, $\mathcal{E}_{\rm ek}$, is color coded along those

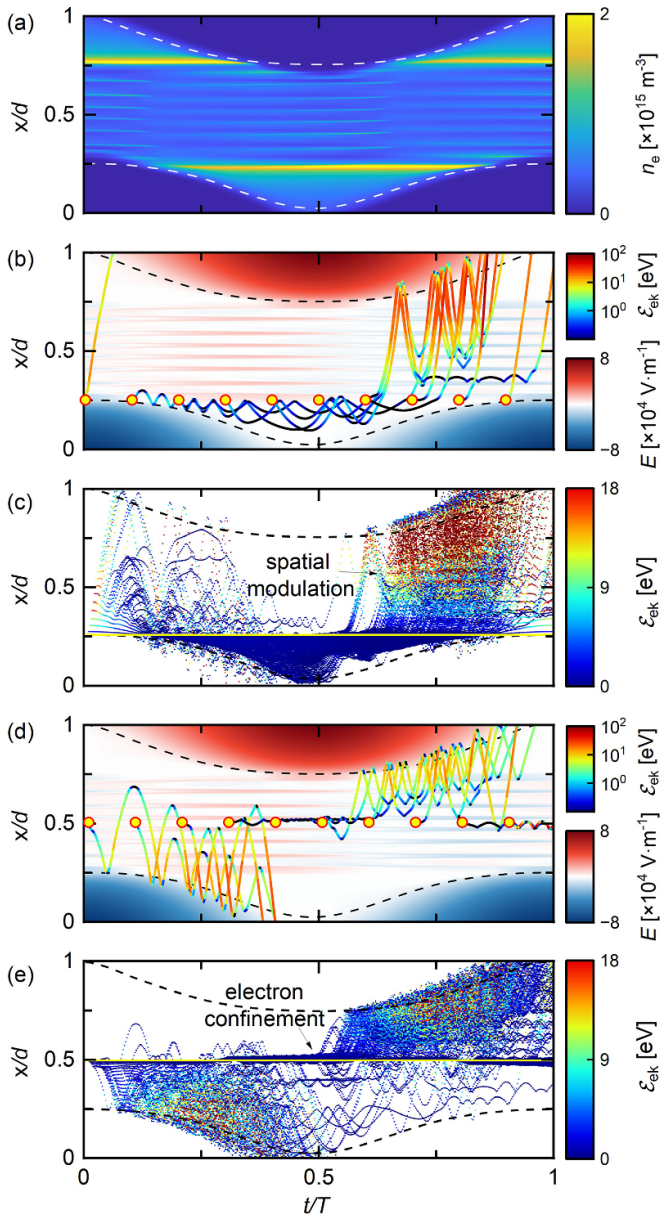


Figure 7. (a) The spatiotemporal distribution of the electron density n_e in case 1. (b) Trajectories of ten test electrons departing at uniform time interval during an RF cycle at the location of $x/d = 0.25$. Kinetic energy, $\mathcal{E}_{ek}$ of those test particles are color coded along the trajectories with logarithmic color bar. (c) $\mathcal{E}_{ek}$ along trajectories of the test electrons that start from $x/d = 0.25$ at 400 different initial phases of an RF cycle. Panels (d) and (e) correspond to panels (b) and (c) respectively, illustrating the trajectories of the test particles departing at $x/d = 0.5$.

trajectories between 0.1 eV and 100 eV as indicated in the logarithmic color bar. In panel (b), the 2nd–6th test electrons are repelled by the electric field in the bulk, and are subsequently reflected by the sheath electric field on the $x/d = 0$ side. After undergoing multiple rebounds between the sheath and bulk region, these test electrons enter another half RF cycle and are accelerated by the spatially modulated field there, traversing through the entire space. The other test electrons, i.e. the 1st and 7th–10th, are accelerated at the beginning, and are absorbed by the boundary after being transported across the entire space. Among all these test electrons, only the 6th is confined, which occurs after its traversing throughout the gap and being reflected by the sheath electric field near $x/d = 1$. None of the other test electrons are confined. As discussed for the green test electron trajectory in figure 5, these electrons can all experience considerable energy absorption, including Ohmic and non-local collisional power absorption, due to their considerable drift velocity and traversing the spatially modulated field. Only a small number of electrons, on the other hand, are confined and undergoes power absorptions. Panel (c) illustrates trajectories of 400 test electrons departing from $x/d = 0.25$, where the corresponding $\mathcal{E}_{ek}$ is drawn using linear levels of color bars, ranging from 0 to 18 eV. Similar to the mechanism introduced in panel (b), test electrons departing at $t/T = 0 \sim 0.5$ are repelled after they enter the bulk region, and undergo rebounds between the sheath and the bulk field. For $t/T = 0.5 \sim 1$, most test electrons can travel through the bulk plasma, and the corresponding kinetic energy exhibits a spatially modulated structure, due to the periodic acceleration and deceleration they undergo in the bulk region. On the other hand, the electron confinement effect is relatively weak. It is worthwhile mentioning that, the spatiotemporal distribution of $\mathcal{E}_{ek}$ in panel (c) shows agreement with $\mathcal{E}_e$ in figure 1(a), which validates the test particle trajectory calculations applied in this work. Figure 7(d) gives trajectories of ten test particles departing from $x/d = 0.5$ and at different initial RF phases. In panel (d), the 4th, 5th, 6th, 9th and 10th test electrons are confined at the beginning, and are accelerated by the spatially modulated electric field as they enter the other half RF cycle then. The other test electrons have been accelerating since their departure. Ultimately, almost all of the test electrons in panel (d) undergo the acceleration process and are able to traverse the spatially modulated field to achieve power absorption. This can be seen more clearly in panel (e). Though some low-energy electrons are initially confined in the bulk region, they subsequently obtain considerable drift velocity and are transported in the bulk plasma. Overall, the enhancement of non-local collisional power absorption in the striation mode is attributed by two reasons. First, the temporal evolution of the spatially modulated field leads to effects similar to sheath oscillation. This ensures that a considerable non-local collision power absorption mechanism exists in the bulk plasma (see figure 6). Second, figures 7(b) and (d) show that the confinement and acceleration processes can occur simultaneously along the same electron trajectory. Most electrons can be transported across the spatially modulated field once confined, ensuring power absorption along trajectories.

4. Conclusion

In conclusion, we have studied the electron dynamics of power absorption in CF_4 capacitive RF discharges. Utilizing the PIC/MCC simulation, in the striation mode, the mean electron energy in the bulk plasma exhibits a spatially modulated

structure where high electron energy peaks can be observed. To investigate the formation of these peaks, we conducted a comparative analysis of electron power absorption via the Boltzmann term analysis method. It was demonstrated that, in the striation mode, the contribution of non-local collisional power absorption surpasses that of Ohmic power absorption in the striated electron energy profile. In contrast, in the DA mode, Ohmic power absorption dominates the electron power absorption process within the entire bulk region. Such enhancement of non-local collisional power absorption can be explained in two aspects. First, the evolution of the spatially modulated field compresses and expands the electron fluid, ensuring the existence of the non-local collisional power absorption mechanism in the bulk plasma. Second, test particle trajectory calculations demonstrate that most electrons can surpass the spatially modulated electric field, ensuring power absorption along their trajectories. Additionally, some low-energy electrons can be trapped in the striated electric field by triggering multiple rebounds, during which negligible power absorption occurs. This confinement eventually leads to the spatially modulated electron density structure.

Data availability statement

The data that support the findings of this study are openly available at the following URL/DOI: https://figshare.com/articles/dataset/Simulation_data_For_striation_mode_CF4_CCP/29 910 212?file = 57 188 708.

Acknowledgments

Z Zhou would like to thank Prof. Y Pu in the Department of Engineering Physics, Tsinghua University, for his valuable suggestions in the title and abstract. This work was supported by the National Natural Science Foundation of China (Grant No. 52250051). The authors also acknowledge financial support from the National Natural Science Foundation of China (No. 52277154), the Beijing Natural Science Foundation of China (Grant No. 3244040), and the Organized Research Support Program (No. YK20240103) from the Department of Electrical Engineering at Tsinghua University. X Wang (Project 327886311) and J Schulze (Project 428942393) acknowledge support of the German Research Foundation. W Zhang also gratefully acknowledges financial support from the China Postdoctoral Science Foundation (Grant No. GZC20231214).

Conflicts of interest

The authors have no conflicts of interest to disclose.

Author contributions

Zhenhua Zhou 0009-0008-3374-5689
Data curation (equal), Formal analysis (equal), Investigation (lead), Methodology (lead), Writing – original draft (lead), Writing – review & editing (equal)

Xiaokun Wang 0000-0003-4160-5316
Data curation (equal), Formal analysis (equal), Methodology (lead), Investigation (lead), Writing - original draft (lead), Writing – review & editing (equal)

Hanyang Li 0009-0009-4903-8089
Investigation (equal), Visualization (equal), Writing – review & editing (supporting)

Dong Yang 0000-0002-8892-7817
Investigation (equal), Visualization (equal), Writing – review & editing (supporting)

Wenjin Zhang 0000-0003-3212-019X
Funding acquisition (equal), Investigation (equal), Methodology (equal), Writing – review & editing (equal)

Julian Schulze 0000-0001-7929-5734
Funding acquisition (equal), Methodology (equal), Visualization (equal), Writing – review & editing (equal)

Peter Hartmann 0000-0003-3572-1310
Data curation (equal), Resources (equal), Software (equal), Writing – review & editing (equal)

Zoltán Donkó 0000-0003-1369-6150
Data curation (equal), Resources (equal), Software (equal), Writing – review & editing (equal)

Yongxin Liu 0000-0002-6506-7148
Writing – review & editing (equal)

Yangyang Fu 0000-0001-9593-3177
Conceptualization (lead), Funding acquisition (equal), Methodology (equal), Supervision (lead), Visualization (equal), Writing – review & editing (equal)

References

[1] Lieberman M A and Lichtenberg A J 2005 *Principles of Plasma Discharges and Materials Processing* (Wiley-Interscience)
[2] Yang D, Verboncoeur J P and Fu Y 2025 *Phys. Rev. Lett.* **134** 045301
[3] Chabert P and Braithwaite N 2011 *Physics of Radio-Frequency Plasmas* (Cambridge University Press)
[4] Makabe T and Petrovic Z 2014 *Plasma Electronics: Applications in Microelectronic Device Fabrication* (CRC Press, Taylor & Francis Group)
[5] Donkó Z, Schulze J, Hartmann P, Korolov I, Czarnetzki U and Schüngel E 2010 *Appl. Phys. Lett.* **97** 081501
[6] Diomede P, Kim D and Economou D J 2013 *AIChE J.* **59** 3214
[7] Wang C, Zhang B, Chen S, Sun Y, Yang X, Peng Y, Chen X and Zhang G 2022 *Plasma Sci. Technol.* **24** 025501
[8] Gao S-H, Gao L-H and Zhou K-S 2011 *Appl. Surf. Sci.* **257** 4945
[9] Gao S-H, Zhou K-S, Lei M-K and Wen L-S 2009 *Plasma Process. Polym.* **6** 530
[10] Wilczek S, Schulze J, Brinkmann R P, Donkó Z, Trieschmann J and Mussenbrock T 2020 *J. Appl. Phys.* **127** 181101
[11] Chabert P, Tsankov T V and Czarnetzki U 2021 *Plasma Sources Sci. Technol.* **30** 24001
[12] Schweigert I V 2004 *Phys. Rev. Lett.* **92** 155001
[13] Kawamura E, Lieberman M A, Lichtenberg A J and Chabert P 2021 *Plasma Sources Sci. Technol.* **30** 35001

[14] Godyak V A and Khanneh A S 1986 *IEEE Trans. Plasma Sci.* **14** 112
[15] Schulze J, Derzsi A, Dittmann K, Hemke T, Meichsner J and Donko Z 2011 *Phys. Rev. Lett.* **107** 275001
[16] Wen H, Schulze J and Zhang Q-Z 2024 *Plasma Sources Sci. Technol.* **33** 034006
[17] Liu Y-X, Donkó Z, Korolov I, Schüngel E, Wang Y-N and Schulze J 2019 *Plasma Sources Sci. Technol.* **28** 075005
[18] Liu Y-X, Korolov I, Schüngel E, Wang Y-N, Donkó Z and Schulze J 2017 *Phys. Plasmas* **24** 073512
[19] Liu Y-X, Korolov I, Schüngel E, Wang Y-N, Donkó Z and Schulze J 2017 *Plasma Sources Sci. Technol.* **26** 55024
[20] Mahdavipour B and Gudmundsson J T 2025 *Plasma Sources Sci. Technol.* **34** 045005
[21] Liu Y X, Schungel E, Korolov I, Donko Z, Wang Y N and Schulze J 2016 *Phys. Rev. Lett.* **116** 255002
[22] Lafleur T, Chabert P and Booth J P 2014 *Plasma Sources Sci. Technol.* **23** 35010
[23] Kaganovich I D, Kolobov V I and Tsendin L D 1996 *Appl. Phys. Lett.* **69** 3818
[24] Masheyeva R, Vass M, Wang X-K, Liu Y-X, Derzsi A, Hartmann P, Schulze J and Donkó Z 2024 *Plasma Sources Sci. Technol.* **33** 045019
[25] Schulze J, Derzsi A and Donkó Z 2011 *Plasma Sources Sci. Technol.* **20** 045008
[26] Brandt S *et al* 2016 *Plasma Sources Sci. Technol.* **25** 045015
[27] Liu G-H, Liu Y-X, Wen D-Q and Wang Y-N 2015 *Plasma Sources Sci. Technol.* **24** 085005
[28] Czarnetzki U and Alves L L 2022 *Rev. Mod. Plasma Phys.* **6** 31
[29] Lafleur T, Chabert P, Turner M M and Booth J P 2014 *Plasma Sources Sci. Technol.* **23** 15016
[30] Lafleur T and Chabert P 2015 *Plasma Sources Sci. Technol.* **24** 44002
[31] Wang X-K, Masheyeva R, Liu Y-X, Hartmann P, Schulze J and Donkó Z 2023 *Plasma Sources Sci. Technol.* **32** 085009
[32] Schulenberg D A, Korolov I, Donkó Z, Derzsi A and Schulze J 2021 *Plasma Sources Sci. Technol.* **30** 105003
[33] Surendra M and Dalvie M 1993 *Phys. Rev. E* **48** 3914
[34] Vass M, Wilczek S, Lafleur T, Brinkmann R P, Donkó Z and Schulze J 2020 *Plasma Sources Sci. Technol.* **29** 85014
[35] Vass M, Wilczek S, Lafleur T, Brinkmann R P, Donkó Z and Schulze J 2020 *Plasma Sources Sci. Technol.* **29** 25019
[36] Schulze J, Donkó Z, Lafleur T, Wilczek S and Brinkmann R P 2018 *Plasma Sources Sci. Technol.* **27** 55010
[37] Vass M, Wilczek S, Lafleur T, Brinkmann R P, Donkó Z and Schulze J 2021 *Plasma Sources Sci. Technol.* **30** 65015
[38] Popov O A and Godyak V A 1985 *J. Appl. Phys.* **57** 53
[39] Godyak V A and Piejak R B 1990 *Phys. Rev. Lett.* **65** 996
[40] Yang D, Wang H, Zheng B, Zou X, Wang X and Fu Y 2023 *Phys. Plasmas* **30** 063510
[41] Yang D, Fu Y, Liu Z, Han X and Fu Y 2024 *IEEE Trans. Plasma Sci.* **52** 4520
[42] Brinkmann R P 2007 *J. Appl. Phys.* **102** 093303